Journal of
Synchrotron
Radiation

ISSN 0909-0495

Received 5 October 2003
Accepted 21 October 2004

A novel BioXAS technique with sub-millisecond time resolution to track oxidation state and structural changes at biological metal centers

Michael Haumann,[a]* Claudia Müller,[a] Peter Liebisch,[a] Thomas Neisius[b] and Holger Dau[a]*

[a]Freie Universität Berlin, FB Physik, Arnimallee 14, D-14195 Berlin, Germany, and [b]ESRF, BP 220, 38043 Grenoble CEDEX, France. E-mail: haumann@physik.fu-berlin.de, holger.dau@physik.fu-berlin.de

Oxidation-state and structural changes at the metal center are crucial for the catalytic reactions of most metalloenzymes. The characterization of reaction intermediates is a prerequisite for understanding the catalytic mechanism. Frequently, intermediates are formed on the microsecond to millisecond timescale. To follow these reactions in real time represents a major challenge in structural biology. Time-resolved BioXAS is a particularly promising tool for resolving such intermediates. A novel approach for BioXAS, termed 'sampling-XAS', is presented. First room-temperature sampling-XAS results have been obtained for the manganese complex of oxygenic photosynthesis. Oxidation-state changes are monitored with a time resolution as good as 200 µs. The current prospects and limitations as well as future perspectives of time-resolved BioXAS are discussed.

Keywords: time-resolved BioXAS; EXAFS; XANES; metalloenzymes; photosystem II.

1. Abbreviations

EXAFS: extended X-ray absorption fine structure.
FT: Fourier transform.
PSII: Photosystem II.
S_i: oxidation states of the Mn complex.
Tyr_Z: redox-active tyrosine residue (D1-Tyr-161) of PSII.
XANES: X-ray absorption near-edge structure.
XAS: X-ray absorption spectroscopy.

2. Introduction

Metalloenzymes play a prominent role in the metabolic pathways of all organisms because an estimated 25–50% of all proteins carry metal atoms at the active sites crucially involved in the catalytic reactions (Hill *et al.*, 1999). Frequently, the catalytic reactions of metalloenzymes can be formulated as a sequence or cycle during which several intermediate states are formed which differ with respect to oxidation state and structure of the metal center. A static picture of the metal center as, for example, determined by crystallography, is often insufficient to understand the mechanism of the catalytic reaction. Essential information on the reaction mechanism is rather expected to result from the detection and characterization of intermediates (Dau & Haumann, 2003). Typically, transitions between such intermediates occur on the microsecond to millisecond time scale. This holds, for example, in the biologically highly important electron transfer chains of photosynthesis and respiration where essentially all involved proteins are metalloenzymes.

Synchrotron radiation techniques have been developed to characterize the structure of reaction intermediates of metalloenzymes at the atomic level as briefly discussed in the following.

(i) Crystallographic methods allow for the determination of complete enzyme structures from X-ray diffraction patterns of protein crystals; information on the electronic structure (oxidation state) of the protein-bound metal center is hardly obtainable. Standard protein crystallography usually provides a static picture of the atomic structure of (metallo)enzymes, now mostly obtained at cryogenic temperatures (around 100 K). The structures of reaction intermediates are accessible, for example, by freeze-quench approaches involving initiation of the reaction sequence, trapping of intermediates, and structure determination by X-ray diffraction. Using state-of-the-art techniques, the study of intermediates which are separated by tens of milliseconds in time may become viable (Stoddard, 2001; Scott, 2002). A method which provides much higher temporal resolution is time-resolved crystallography (Moffat, 2003). This method relies on the observation of structural changes in crystals positioned in the X-ray beam by recording time-series of diffraction patterns using short X-ray pulses before and after the onset of a reaction. By employing sudden trigger events (*e.g.* laser-flash excitation) for initiation

of the reaction and by variation of the delay time between trigger and X-ray pulse, the determination of individual structures which are separated by time intervals of only picoseconds becomes feasible. This experiment requires high-quality crystals and reactions which can not only be rapidly initiated (by laser-pulse excitation) but also repetitively initiated to limit the amount of required crystals. The requirement of rapid and complete relaxation limits the application range of this approach. Impressive results using time-resolved crystallography have been obtained from studies of photochemically inducible reactions occurring in the subnanosecond time domain (Ren *et al.*, 2001; Schotte *et al.*, 2003; Adachi *et al.*, 2003).

(ii) By using XAS, information on both the atomic structure and the oxidation state of the metal center becomes available {Teo, 1986; Yachandra, 1995; Scott, 2000; Dau *et al.*, 2003; for a recent review, see the special issue on BioXAS [*J. Synchrotron Rad.* (2003). **10**, 1–112]}. It represents a specific advantage of XAS that experiments can be performed on proteins in solution. Structural and electronic changes during a catalytic reaction cycle have been addressed by the three alternative BioXAS methods (Ascone *et al.*, 2003; Dau & Haumann, 2003) discussed below.

(*a*) Stopped-flow/freeze-quench approaches can be used to populate reaction intermediates of metalloenzymes at ambient temperatures; XAS spectra are subsequently collected at cryogenic temperatures. Using this technique, XANES and EXAFS spectra during a single substrate turnover of the zinc site of bacterial alcohol dehydrogenase, separated by only $\sim$3 ms in time, have been obtained (Kleifeld *et al.*, 2003). We (Iuzzolino *et al.*, 1998; Dau *et al.*, 2001; Dau & Haumann, 2003; Dau *et al.*, 2003) and others (Ono *et al.*, 1992; Robblee *et al.*, 2001) have extensively used a related technique: the flash-freeze approach (population of intermediates by flash excitation of samples at ambient temperatures followed by rapid freezing and XAS data collection at cryogenic temperatures) to investigate the structural and oxidation state changes of the manganese complex of photosynthesis during its catalytic cycle (see below).

(*b*) In dispersive-XAS, a 'white' X-ray beam is resolved into a continuum of beams of different 'colours' (or energies) by a dispersive crystal and refocused on the sample. Thereby, the incidence angle on the sample becomes energy-dependent so that, behind the sample, the individual energies of the transmitted X-rays can be monitored simultaneously by a spatially resolving detector (Pascarelli *et al.*, 1999). In principle, this technique can provide high time resolution. Dispersive-XAS, however, requires large metal concentrations (>10 m*M*) in the sample which are rarely obtainable with biological material. Accordingly, only few examples of dispersive-XAS on metalloenzymes have been reported (Joo *et al.*, 1990; Della Longa *et al.*, 1994).

(*c*) Rapid-scan XAS techniques are a promising tool for studying state transitions at biological metal centers under physiological conditions where catalysis can proceed (*e.g.* protein in solution, room temperature). XAS spectra are collected by means of rapid and continuous scans of the monochromato r; if required, the undulator gap is synchronously scanned (Solé *et al.*, 1999). Using piezo-electric control of the monochromator (piezo-quick-EXAFS), XANES spectra have been obtained within $\sim$50 ms on relatively dilute samples (<10 m*M* metal concentration) and in fluorescence mode (Lützenkirchen-Hecht *et al.*, 2001; Richwin *et al.*, 2001). Using the rapid-scan mode (synchronous scan of monochromator and undulator gap) of beamline ID26 at the ESRF (Grenoble) we have obtained room-temperature EXAFS spectra of the manganese complex of photosynthesis within minimally 3 s of scan time (for a $\sim$600 eV scan) after the laser-flash excitation which induces a state transition (Haumann *et al.*, 2001; Haumann, Grabolle *et al.*, 2002; Haumann, Pospisil *et al.*, 2002; Dau & Haumann, 2003; see below).

By the X-ray techniques discussed above, it has not been possible to follow changes in the electronic and atomic structure of biological metal centers of dilute non-crystalline protein samples (metal concentration $\lesssim$ 1 m*M*) in the microsecond time domain, a time range that comprises most of the electron and proton transfer reactions that are the basis for the function of many metalloenzymes.

Today, to counteract radiation damage, structural synchrotron studies often involve deeply frozen enzymes. Whether the cryo-structures deviate from the ones at physiological temperatures is often uncertain (see Shimizu *et al.*, 2000). Temperature-dependent XAS measurements revealed changes in the structural dynamics of metal sites above the so-called 'glass-transition point' ($\sim$200 K) of proteins (Scherk *et al.*, 2001; Dau *et al.*, 2004). Real-time BioXAS techniques should avoid such ambiguities and facilitate monitoring of the state transitions under physiological conditions (meaning at ambient temperatures and on proteins in an aqueous environment).

The tetra-manganese complex of PSII catalyses the light-driven production of dioxygen from two water molecules. This reaction is of outstanding biological importance because it provides most of the oxygen in the atmosphere [for a recent review see the special issue on photosynthetic water oxidation, *Biochim. Biophys. Acta*, (2001), **1503**]. Despite the availability of a wealth of structural information from recent crystallographic data (Zouni *et al.*, 2001; Kamiya & Shen, 2003; Ferreira *et al.*, 2004) and from previous XAS investigations (for review see Dau *et al.*, 2001; Robblee *et al.*, 2001; Dau *et al.*, 2003), the mechanism of water oxidation is still insufficiently understood (Rutherford & Faller, 2001). The reaction cycle of water oxidation is specifically well suited for the development of time-resolved XAS techniques as it comprises four intermediate states (S_0, S_1, S_2, S_3) of the Mn complex which can be populated by flash excitation of PSII samples and which are stable at room temperature on the seconds to minutes time scale. Starting from the dark-stable S_1 state, two flashes of light, each causing the abstraction of an electron from the Mn complex thereby inducing a transition $S_i \rightarrow S_{i+1}$, drive the system to the S_3 state. Upon the third flash, transition $S_3 \rightarrow S_0$ is initiated. This reaction involves the transient formation of a (hypothetical) intermediate state, S_4, which spontaneously converts to S_0 under release of dioxygen (Haumann & Junge,

1999). It has been shown by various spectroscopic techniques that the time course of electron abstraction depends on the number of oxidizing equivalents already stored on the Mn complex; half-rise times of about 30 µs, 100 µs, 300 µs and 1.2 ms have been reported for the transitions $S_0 \rightarrow S_1$, $S_1 \rightarrow S_2$, $S_2 \rightarrow S_3$ and $S_3 \rightarrow S_0$, respectively (Dekker *et al.*, 1984; Renger & Hanssum, 1992; Haumann, Bögershausen *et al.*, 1997; Haumann, Hundelt *et al.*, 1997). The reaction cycle of water oxidation is schematically summarized in Fig. 1.

Previous XAS investigations are suggestive that the Mn complex is organized in two pairs of di-μ-oxo-bridged Mn pairs in the S_1 state (Yachandra *et al.*, 1987; Dau *et al.*, 2001; Pospisil *et al.*, 2003; Dau *et al.*, 2003). Investigations by our group (Iuzzolino *et al.*, 1998; Dau *et al.*, 2004; Haumann *et al.*, 2004) revealed that Mn-centered oxidation is likely to occur on each oxidizing transition. [Different interpretations have been offered by others (Messinger *et al.*, 2001); for a detailed discussion see Dau *et al.* (2003).] Furthermore, accompanying structural changes (*e.g.* changes in the bridging mode between the four Mn atoms on at least some of the S transitions) have been postulated on the basis of XAS results (Liang *et al.*, 2000; Dau *et al.*, 2001; Robblee *et al.*, 2002; Dau & Haumann, 2003; Magnuson *et al.*, 2004).

In this work, a novel XAS technique for following changes in the electronic and atomic structure of biological metal centers is presented, allowing the study of state transitions in real time, at room temperature, and in water-containing samples. We have termed this approach 'sampling-XAS'. The perspectives of time-resolved sampling-BioXAS are discussed.

3. Materials and methods

Oxygen-evolving PSII-enriched membrane particles (~1200–1400 µmol O_2 mol^{-1} chlorophyll h^{-1}, measured at 301 K) with the Mn complex in its S_1 state were prepared with betaine as stabilizer as described by Iuzzolino *et al.* (1998), Schiller *et al.* (1998) and Schiller & Dau (2000). The PSII XAS samples were prepared by a novel drop-and-dry technique: the sample holders were strips of black polycarbonate (1 mm × 20 mm × 200 mm) with ten cavities (15 × 2 mm holes backed by Kapton tape of 20 µm thickness; 15 mm spacing between the cavities). The artificial electron acceptor PPBQ was added to a solution of PSII membrane particles (~7–8 mg chlorophyll mL^{-1}; 200 µM PPBQ). Then, the suspension was pipetted into the cavities of the sample holder. Loaded sample holders were partially dried in a desicator at ~3 × 10^7 Pa air pressure for 2 h at 277 K over silica gel (in darkness). The PSII-filled sample holders were prepared at the synchrotron radiation source immediately before the start of the X-ray experiment. Each of the more-than-1000 samples used in the experiments contained about 200 µg of chlorophyll and Mn at a concentration of ~1 m*M*.

X-ray absorption measurements at the Mn *K* edge were performed at the undulator beamline ID26 of the European Synchrotron Radiation Facility (ESRF) in Grenoble (France). A Si 220 crystal monochromator was used, detuned to 70% of maximal intensity. The X-ray fluorescence was monitored by a photodiode (active area ~4 cm^2) shielded by thin Cr- and Al-foil filters against scattered X-rays and visible light. The PSII samples were surrounded by plain air (room temperature of 291 K; angle of 55° between sample normal and electric field vector of the X-ray beam). One scan per sample was performed on dark-adapted samples (X-ray spot size of 1 mm × 1 mm). For further details see Solé *et al.* (1999), Meinke *et al.* (2000), Haumann, Grabolle *et al.* (2002), Haumann, Pospisil *et al.* (2002) and Dau & Haumann (2003).

Rapid-scan XAS data evaluation was carried out as described elsewhere (Meinke *et al.*, 2000; Haumann, Grabolle *et al.*, 2002; Haumann, Pospisil *et al.*, 2002). Energy calibration was facilitated by using the narrow pre-edge peak of a simultaneously measured $KMnO_4$ absorption spectrum as a standard (peak at 6543.3 eV). The Mn *K*-edge energy was determined using the 'integral method' described by Dittmer *et al.* (1998) and Dau *et al.* (2003).

Flash excitation of the samples was performed at ID26 by a frequency-doubled Q-switched Nd-YAG laser (Quantel Brilliant, FWHM 5 ns, 532 nm, ~150 mJ per flash). Guided by appropriate laser optics, the light flashes illuminated both sides of the samples simultaneously [see Fig. 7 of Dau & Haumann (2003)].

During the XAS experiments, the sample holders containing ten PSII samples were positioned with a precision of ~4 µm in the X-ray beam by a home-built computer-controlled sample changer (linear stage with 15 cm driving range and stepping motor) which allows for sample exchange

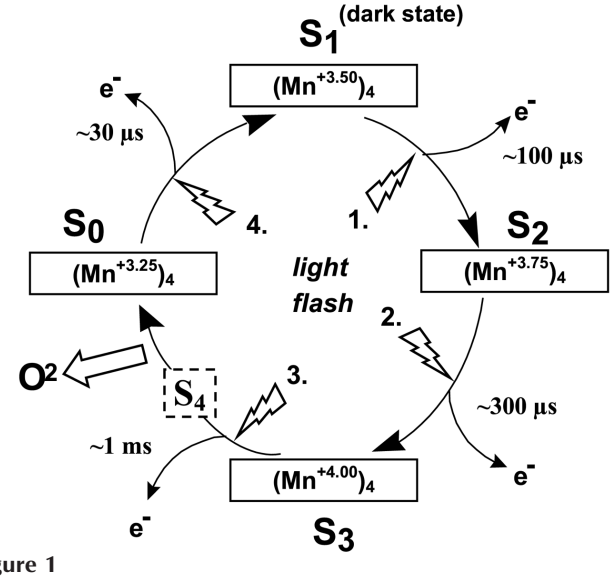

Figure 1
Simplified scheme of the catalytic cycle of water oxidation at the tetra-manganese complex of photosystem II. The S_1 state is dark-stable. Application of one, two or three laser flashes results in the predominant population of S_2, S_3 and S_0, respectively. The individual S states are acquired after the respective laser flash with the specified half-rise times. The indicated average oxidation states of the four Mn ions in the semistable S states follow the assignments made by Dau *et al.* (2003). The S_4 state is assumed to be transiently formed after the third flash. Its spontaneous conversion to the S_0 state is coupled to the release of dioxygen.

within ~3 s. Only the sample exposed to the X-ray beam was accessible to the laser flashes; neighbouring samples were shielded against illumination.

Two types of experiments were performed. (i) XAS scans using the rapid-scan mode of ID26 (synchronous scan of undulator gap and monochromator) were performed within 3 s (scan range 6500–7100 eV). (ii) Time scans of fluorescence were carried out at a fixed X-ray energy and measuring the X-ray fluorescence intensity as a function of time using either the beamline electronics for data acquisition (10 or 20 ms per data point) or a personal computer equipped with an A/D card (200 μs per data point, 10 kHz electrical bandwidth). A rapid beam shutter ($t_{open} \simeq 10$ ms) opened immediately before the start of data collection. All experiments were carried out at room temperature.

4. Results and discussion

4.1. The sampling-XAS technique

The used method of sampling-XAS at room temperature involves the following experimental protocol (Fig. 2). (i) To yield a reference spectrum of the Mn complex in its S_1 state, a rapid EXAFS scan was performed within 3 s on a first spot of a PSII sample (not illuminated by laser flashes) (Fig. 2-i). (ii) Then, the sample was repositioned to expose a second spot to the X-ray beam. After repositioning, the time course of the X-ray fluorescence intensity was monitored at a fixed excitation energy for 60 s [time scan of fluorescence (Haumann, Grabolle *et al.*, 2002; Haumann, Pospisil *et al.*, 2002)] (Fig. 2-ii). During the first few seconds of the time scan, three nanosecond laser flashes illuminated the sample, causing the stepwise advancement of the Mn complex through the whole catalytic cycle (inset in Fig. 2-ii, arrows). (iii) Thereafter, on the same sample spot a rapid EXAFS scan was performed (Fig. 2-iii). Then, a new sample was exposed to the beam and the whole sequence of measurements started again. Eventually, the used excitation energy during the time scan was changed to a new value.

Each flash given to the PSII samples during the time scans caused a jump in the fluorescence intensity level (Fig. 2-ii, inset). These jumps are indicative of the stepping of the Mn complex through its catalytic cycle. They originate in the S-state dependence of the XAS spectra of the Mn complex. Differences are most pronounced in the edge region (see Fig. 2-ii, inset) because of the different *K*-edge positions of the individual S states; in the EXAFS region, the observable differences are smaller (not shown). The rise of the fluorescence intensity within 60 s (Fig. 2-ii) is attributable to the photoreduction of the high-valent Mn_4 complex to four Mn(II) ions resulting from the creation of numerous radicals in the sample by X-ray irradiation (Dau *et al.*, 1997; Meinke *et al.*, 2000; Haumann, Grabolle *et al.*, 2002). The magnitude of this rise reflects the difference in the spectra taken before (S_1 state, Fig. 2-i) and after the time scan [Mn(II) spectrum, Fig. 2-iii].

To construct XAS spectra at selected points in time from fluorescence time scans at a series of energies, the following procedure is used:

(*a*) For the excitation energy, E, used in the time scan, the fluorescence offset, $F_{off}(E)$, and the magnitude of the edge jump, F_{norm} (independent of E), were determined from the XAS scan measured on the same sample spot after the time scan (Fig. 2-iii).

(*b*) Using these parameters, the fluorescence time-scan trace (Fig. 2-ii) was normalized to yield the calibrated fluorescence $F_{cal}(E, t)$ according to

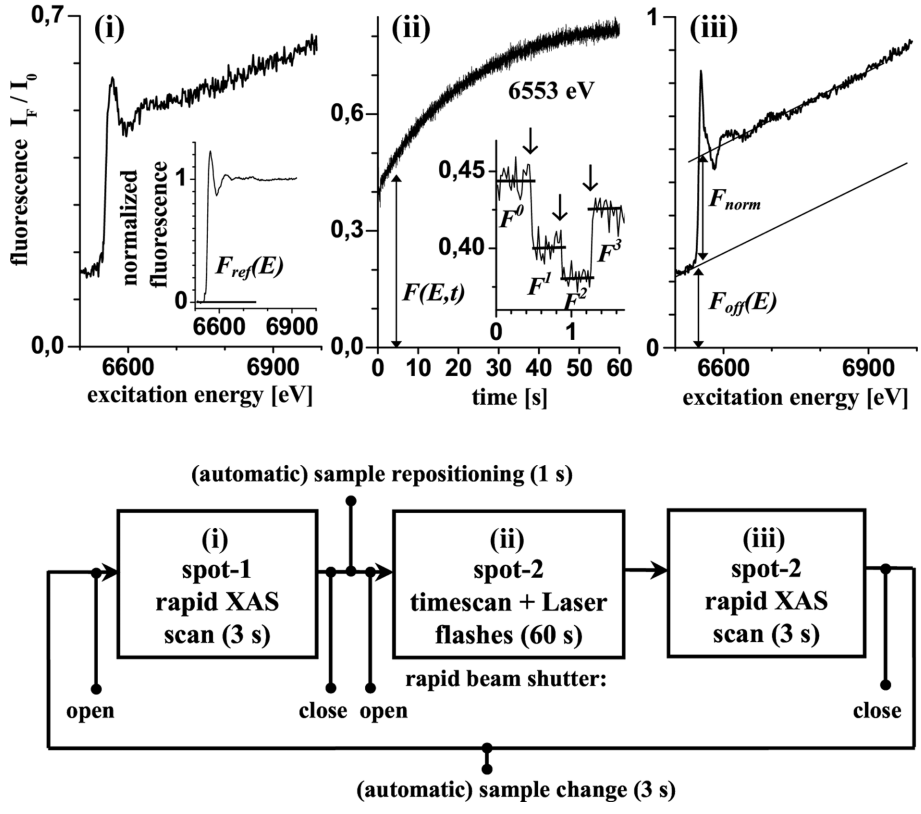

Figure 2
The experimental procedure of sampling-XAS. (i) Rapid-scan XAS reference spectrum of the Mn complex in its S_1 state (no flash illumination, scan duration 3 s). The inset shows the S_1-state spectrum after averaging of several scans from a series of experiments and normalization. (ii) Time scan of fluorescence at 6553 eV (in the rising part of the Mn *K* edge) at a resolution of 10 ms per point (single-scan data). The inset shows the first 1.7 s where three laser flashes have been fired (arrows). (iii) Rapid-scan XAS spectrum measured after the time scan. The meaning of the indicated fluorescence-intensity levels and further details are explained in the text. The lower picture summarizes the sequence of measurements in the sampling-XAS experiment schematically. The X-ray beam was blocked between the data-collection periods by a rapid beam shutter.

$$F_{\rm cal}(E,t) = F(E,t)/F_{\rm norm} - F_{\rm off}(E)/F_{\rm norm}. \quad (1)$$

(*c*) Plotting the values of $F_{\rm cal}$ at a certain point in time during the time scans against the respective excitation energies E should yield the XAS spectrum.

The above-described method is precise enough to obtain sound sampling-XANES spectra (see below). In the EXAFS region, the fluorescence changes during the time scan are much smaller, *i.e.* a higher precision of the calibration is required. We find that $F_{\rm norm}$ can be determined to a high precision whereas the determination of $F_{\rm off}$ by the above procedure introduces a significant error. Therefore, to obtain sampling-EXAFS spectra, we use the normalized S_1-state reference spectrum (inset in Fig. 2-i) for calibration of time-scan data. For a perfectly precise value of $F_{\rm off}(E)$, the calibrated fluorescence levels, $F_0^{\rm cal}(E)$, attributable to the Mn complex in the S_1 state [obtained from fluorescence levels $F^0(E)$ before flash excitation, see inset of Fig. 2-ii] and the fluorescence levels $F_{\rm ref}(E)$ of the normalized S_1-state reference spectrum (inset in Fig. 2-i) are identical; the S_1-state sampling-XAS and rapid-scan spectra should be equal,

$$F_{\rm cal}^0(E) = F_{\rm ref}(E). \quad (2)$$

To ensure validity of (2), we now replace the $F_{\rm off}(E)$ values in (1) by the following expression,

$$F_{\rm off}(E) = F^0(E) - F_{\rm ref}(E)\,F_{\rm norm}, \quad (3)$$

yielding (4) which is used to calculate the refined calibrated fluorescence values, $F_{\rm cal}^r(E)$, at each energy point,

$$F_{\rm cal}^r(E,t) = F_{\rm ref}(E) + \Delta F(E,t) \quad (4)$$

with

$$\Delta F(E,t) = \frac{F(E,t) - F^0(E)}{F_{\rm norm}}.$$

In the present study, the spectrum of the dark-stable S_1 state is used as a reference spectrum. Equation (4) simply means that the changes induced by the laser-flash illumination are normalized and added to the reference spectrum. Plotting $F_{\rm cal}^r$ against the respective excitation energies at each point in time should yield refined sampling-XAS spectra. In the following, complete sampling-XANES spectra derived according to (1) and sampling-EXAFS spectra calculated using (4) of the Mn complex of PSII are presented.

4.2. Time scans and sampling-XANES on the Mn complex of PSII to follow radiation damage

One problem of XAS measurements on metalloenzymes at room temperature is that the rate of radiation damage is drastically increased compared with measurements at cryogenic temperatures (Meinke *et al.*, 2000; Haumann, Grabolle *et al.*, 2002; Grabolle *et al.*, 2005). This problem is even more severe in the case of highly oxidized metal centers where rapid X-ray reduction of the metal may occur. An example of this effect is depicted in Fig. 3(*a*) where the rise in fluorescence to the constant level reached after about 60 s reflects the reduction of the majority of the highly oxidized Mn atoms (average oxidation state of +3.5 in the S_1 state) to the Mn(II) level. The rise shows a lag phase of ∼3 s duration. A similar lag has been previously observed with samples initially in the S_1 state (Haumann, Grabolle *et al.*, 2002; Haumann, Pospisil *et al.*, 2002). Its length depends on the X-ray flux; longer lag phases are obtained at lower X-ray intensities (Haumann, Grabolle *et al.*, 2002; Haumann, Pospisil *et al.*, 2002).

Fig. 3 shows sampling-XANES spectra (symbols) that were constructed from time scans measured on dark-adapted samples (Mn in the S_1 state). The shown spectra correspond to X-ray irradiation intervals ranging from 0 to 60 s. These spectra have been obtained employing equation (1); no reference spectrum was involved. The sampling-XANES

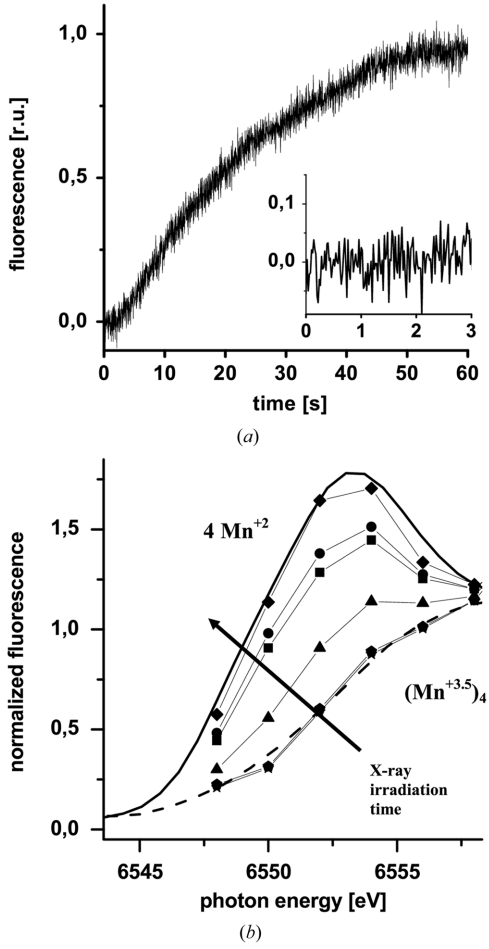

Figure 3
Time course of X-ray photoreduction. (*a*) Time scan of fluorescence at 6552 eV on a dark-adapted PSII sample (Mn complex in the S_1 state). The rise shows a lag phase with a duration of ∼3 s. Inset: the first three seconds of the main trace. (*b*) Sampling-XANES spectra of the Mn complex (symbols) before, during and after X-ray irradiation for 60 s. Spectra have been obtained by averaging over 300 ms of time-scan data as in (*a*) immediately after the onset and after 3, 10, 25, 30 and 60 s of X-ray irradiation (arrow). The lines represent a normalized rapid-scan spectrum of the S_1 state (dashes) (see Fig. 2-i, inset) and a normalized spectrum attributable to hexaquo Mn(II) (solid line) as obtained after the time scan by a rapid EXAFS scan on the same spot (see Fig. 2-iii). For the normalized rapid-scan spectra, 25–30 individual scans have been averaged.

spectra closely resemble those that have been obtained by rapid-scan XAS (lines in Fig. 2) before (Mn complex in its S_1 state) and after [Mn(II) spectrum] the time scans (compare Figs. 2-i and 2-iii). The spectrum obtained after 3 s is still similar to that obtained immediately after the onset of X-ray irradiation (edge shift to lower energies of less than 0.1 eV). Thus, if the full length of the lag phase is used for rapid EXAFS scans, the Mn complex remains essentially (>90%) in the S_1 state. The sampling-XANES spectra obtained for longer X-ray irradiation clearly show changes in shape and edge energy owing to the formation of increasing amounts of Mn(II) in the samples upon the destruction of the two di-μ-oxo-bridged Mn pairs (Grabolle *et al.*, 2005) by photoreduction of Mn in the tens of seconds time range.

4.3. Sampling-XANES on the Mn complex in different S states

From time scans of the fluorescence intensity during a laser-flash illumination sequence (see Fig. 2), the stepping of the Mn complex through its catalytic cycle is monitored. When this technique is applied in the region of the Mn *K* edge, even small changes in the XANES spectra of the four intermediate states become directly visible. Such changes are less reliably observed by continuous-scan XAS techniques (uncertainty in the normalization of the spectra by a few percent already may render the detection of small differences unreliable). This specific benefit of the time-scan technique is demonstrated by the data in Fig. 4. As a particularly interesting example we discuss the changes induced by flashes 1 and 2 populating the S_2 and S_3 states, respectively. At the various excitation energies very different relative changes of the fluorescence intensities are observed on flashes 1 and 2 (Fig. 4). As can be deduced from Fig. 4, the change in fluorescence is negative on flash 1 but positive on flash 2 in the region of the pre-edge peak (around 6545 eV, compare Fig. 5). Flashes 1 and 2 induce an approximately equal decrease in fluorescence at 6549.5 eV. At 6552.8 eV, the decrease is clearly larger on flash 1 than on flash 2. At 6559 eV, flash 1 induces a decrease whereas flash 2 results in an increase of fluorescence. Beyond the edge maximum (at 6571 eV) both flashes 1 and 2 induce an increase of the fluorescence intensity. A decrease of the fluorescence in the rising part of the edge is indicative of a shift of the edge position to higher energies. If only the edge energy increases but the edge shape remains unchanged, one expects a fluorescence decrease in the whole rising part of the edge upon a flash. Now, translating the fluorescence changes in Fig. 4 into changes of the XANES spectra, we note that the edge spectrum of the S_3 state shifts to higher energies mostly in its part roughly below the half-height, whereas the S_2-state edge is shifted to higher energies with respect to the S_1 edge in its whole rising part. A crossover between the S_3-state and S_2-state spectra is observed at around 6556 eV. Above this energy, the S_3 edge is higher. On the basis of simulations using modern full-multiple scattering code (Ankudinov *et al.*, 1998), we have previously attributed the changes in the shape and energy position of the S_3-state XANES to the formation of six-coordinated Mn(IV) from five-coordinated Mn(III) occurring upon the $S_2 \rightarrow S_3$ transition (Dau *et al.*, 2003). The time-scan data in Fig. 4 provide a first indication that similar changes in the XANES are observed in cryo- and room-temperature XAS measurements [for low-temperature data see Iuzzolino *et al.* (1998), Messinger *et al.* (2001), Dau *et al.*, 2003)].

Sampling-XANES spectra of the dark-stable S_1 state and of the sample predominantly in the S_2 state were constructed [according to (1)] from time scans using the average fluorescence intensities before and after the first flash given to PSII

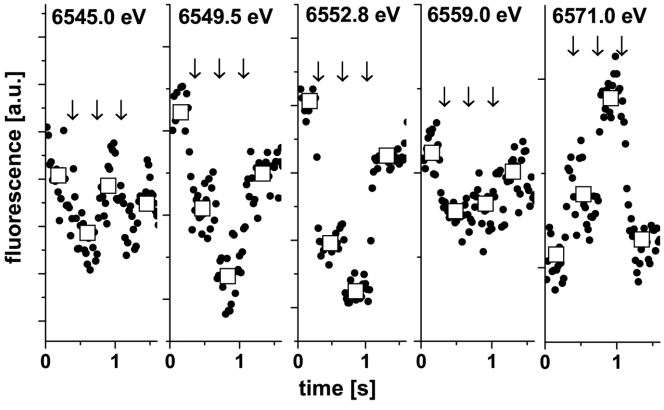

Figure 4
Time scans of X-ray fluorescence at various excitation energies during laser-flash illumination of the Mn complex. The flash spacing was 400 ms. For these traces, 13 to 34 transients were averaged, which have been measured in non-overlapping excitation energy intervals of ±1–3 eV around the indicated mean energies. The time resolution was 20 ms per point. Traces are not normalized and plotted on different scales for better comparison. Squares denote the average fluorescence levels before and after the laser flashes. The arrows indicate the application of a laser flash.

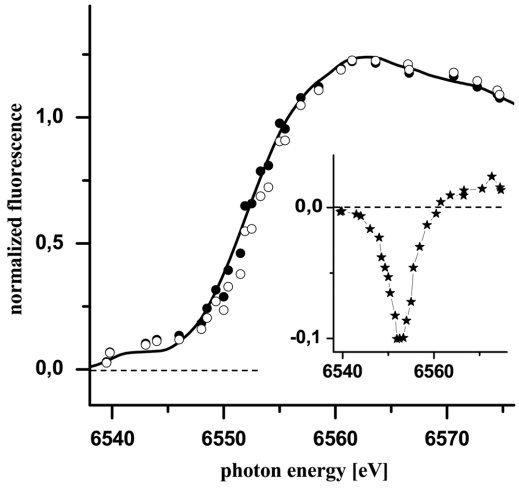

Figure 5
Sampling-XANES spectra of the Mn complex at room temperature before (solid circles) and after (open circles) the first laser flash (predominant population of the S_1 and S_2 states, respectively). Spectra were obtained from time-scan traces (averaging of 5–9 scans at each energy point) according to equation (1) in the text. The points represent the fluorescence intensities averaged over approximately 400 ms before and after flash illumination (F^0 and F^1 levels in Fig. 2-ii). XANES spectra have been slightly smoothed by adjacent averaging over two data points for better comparison. The line represents the rapid-scan S_1-state reference spectrum. Inset: one-flash minus zero-flash difference spectrum.

samples (F^0 and F^1 levels in the inset of Fig. 2-ii). The resulting spectra (Fig. 5, symbols) are significantly affected by noise contributions and represent a preliminary result. We note that these spectra correspond to data obtained within only 400 ms either before or after the laser flash. The thus obtained pre-flash sampling-XANES spectrum (solid circles) seems to be in agreement with the S_1-state reference spectrum obtained by rapid-scan XAS (Fig. 5, line). After the flash, the *K* edge is shifted to higher energies (most clearly seen in the inset of Fig. 5 which shows the difference of one-flash minus the zero-flash spectrum); an upshift in energy by ~0.7 eV is estimated at half-height. This upshift reflects the oxidation of the Mn complex by one equivalent owing to electron abstraction in the $S_1 \rightarrow S_2$ transition (Yachandra *et al.*, 1987; Messinger *et al.*, 2001; Iuzzolino *et al.*, 1998; Haumann, Pospisil *et al.*, 2002; Dau *et al.*, 2003). The roughly derivative-like difference spectrum, which crosses the zero line at an energy of ~6561 eV (inset in Fig. 5), suggests that the *K*-edge shape is similar in S_1 and S_2; the edge position, however, is shifted to higher energies in S_2. These observations are compatible with the notion that no major structural changes are coupled to the single-electron oxidation of Mn on the $S_1 \rightarrow S_2$ transition.

4.4. First sampling-EXAFS spectra to monitor structural changes in the Mn complex

From similar data as shown in Figs. 2 and 4, but extending over the EXAFS region, first sampling-EXAFS spectra of the Mn complex in its S_1 state (no flash illumination), after one laser flash (predominant population of the S_2 state) and after two flashes (predominant S_3 population) were constructed according to (4) using the continuous-scan S_1-state spectrum (Fig. 2-i) as a reference. The resulting sampling-EXAFS oscillations are shown in the inset of Fig. 6. Two prominent peaks are obvious in the FTs of the EXAFS oscillations (Fig. 6). Owing to noise level and limited *k*-range, only a tentative interpretation can be given. Peak I is attributed to a first sphere of mainly oxygen ligands to Mn whereas peak II mainly results from Mn → Mn interactions of ~2.7 Å length, attributable to pairs of di-μ-oxo-bridged Mn atoms as discussed elsewhere (Penner-Hahn, 1999; Robblee *et al.*, 2001; Dau *et al.*, 2001). Peaks I and II behave differently when advancing in the S-state cycle. Peak I increases on the first and second flash. Peak II is about equal in the zero- and one-flash spectra but significantly increased in the two-flash spectrum. Qualitatively very similar changes in the Fourier-transformed spectra have been previously observed in EXAFS spectra measured at 20 K (freeze-quench approach) (Dau *et al.*, 1998, 2001; Haumann *et al.*, 2001, 2004) and at room temperature (rapid-scan approach; laser-flash illumination of samples exposed to the X-ray beam) (Haumann *et al.*, 2001, 2004; Haumann, Grabolle *et al.*, 2002). The increase of the magnitude of FT peak II in the two-flash spectrum has been interpreted as indicating the formation of a new di-μ-oxo bridge between Mn ions in the S_3 state (Dau *et al.*, 2001; Haumann *et al.*, 2004). Pure spectra of the S states can be obtained by deconvolution techniques. As shown elsewhere (Dau *et al.*, 2001; Haumann *et al.*, 2004), deconvolution leads to enhancement of the differences already visible in the raw spectra of Fig. 6.

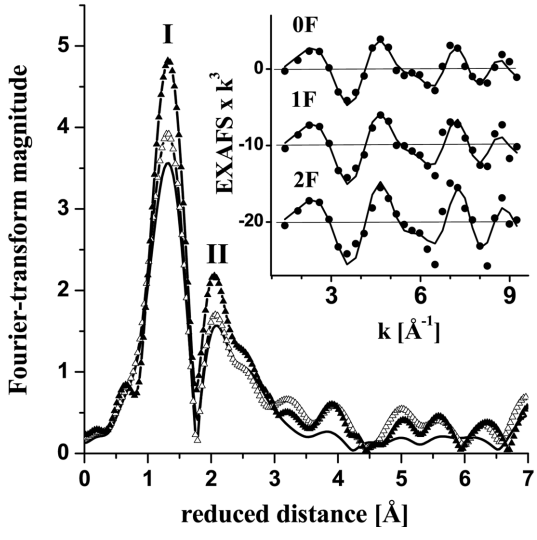

Figure 6
Inset: room-temperature EXAFS oscillations (experimental data, dots) obtained by the sampling-XAS approach of the Mn complex predominantly in states S_1 (no flash, 0F), S_2 (one flash, 1F) and S_3 (two flashes, 2F). Spectra have been obtained from time scans in the EXAFS region by averaging the fluorescence intensity over 200 ms before and after the laser flashes (flash spacing 200 ms). Lines have been drawn to guide the eye. The main picture shows the respective FTs (solid line, 0F; white triangles, 1F; black triangles, 2F). FTs have been calculated from EXAFS oscillations ranging over 10–350 eV above E_0 (6547 eV) and using cosine windows extending over 10 and 25% at the low-*k* and high-*k* side, respectively, of the k^3-weighted data.

4.5. First steps towards the tracking of state transitions with microsecond time resolution

In principle, the time resolution of the sampling-XAS technique can also be extended into the microsecond (or even nanosecond) range. Measuring time scans of fluorescence with microsecond resolution may allow monitoring of, in real time, the transitions of the metal center between the intermediate states of its catalytic cycle. Fig. 7 shows a time scan of fluorescence at 6553 eV (dots) with a resolution of 200 µs per point. The shown transition was initiated by the third laser flash which mainly induces the oxygen-evolving $S_3 \rightarrow S_0$ step.

On the $S_3 \rightarrow S_0$ transition, Mn is reduced by electrons from the bound water resulting in the formation of dioxygen. Consequently, the Mn *K* edge shifts to lower energies causing a fluorescence increase in the *K*-edge region upon flash 3 (see Fig. 2-ii, inset). The fluorescence transient on flash 3 (Fig. 6) clearly reveals several points in its rising part. A single-exponential fit of the data yields a rise time of $t_{1/2}$ = 1.1 ms (line). Very similar rise-time values are typically observed by other techniques such as optical absorption spectroscopy and EPR which have been used to study the kinetics of Mn oxidation or Tyr_Z^{ox} reduction (Rappaport *et al.*, 1994; Haumann, Hundelt *et al.*, 1997; Razeghifard & Pace, 1997). The rise time is found to be slower in preparations with less-

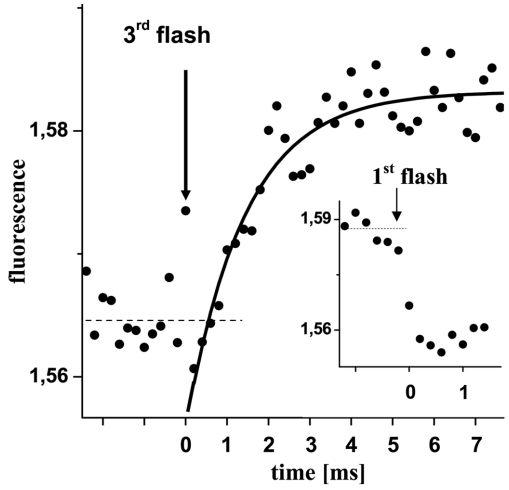

Figure 7
Monitoring of the $S_3 \rightarrow S_0$ transition with microsecond resolution by X-ray fluorescence time scans. Main trace: time course of fluorescence (dots) induced by the third flash (arrow) at an excitation energy of 6553 eV (obtained by averaging of 46 transients measured within an interval of ± 2 eV around the mean energy of 6553 eV at a resolution of 200 µs per point). The line represents a single-exponential fit to the data with $t_{1/2} = 1.1$ ms. The fit-curve starts below the fluorescence level before the flash (dashes). This is explainable by contributions from centers still in the S_2 state prior to the flash. [When these centers undergo the $S_2 \rightarrow S_3$ transition upon the third flash, they cause a rapid decrease in the X-ray fluorescence (compare Fig. 2-ii).] Inset: transient at 200 µs per point observed upon the first flash inducing the $S_1 \rightarrow S_2$ transition.

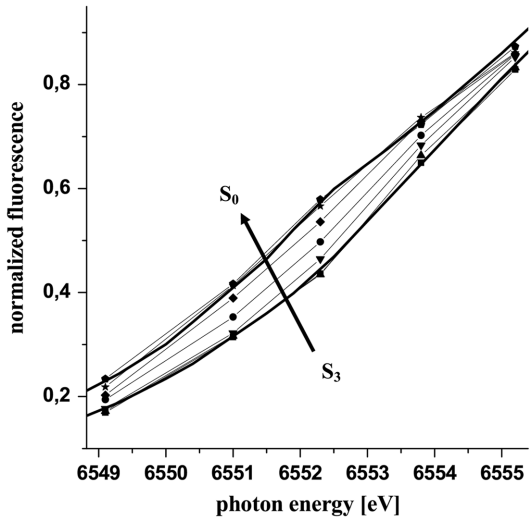

Figure 8
Transient spectra of the $S_3 \rightarrow S_0$ transition. Spectra (symbols and thin lines) have been obtained from fluorescence changes induced by flash 3 measured at a time resolution of 200 µs per point (see Fig. 7). At each energy point, up to 35 time scans measured in an interval of ± 1 eV around the indicated mean energy have been averaged. The shown sampling-XANES spectra were obtained within 500 µs before the flash and within six intervals of 500 µs length, the first one starting immediately after the flash and the last one extending up to 3 ms (arrow). The strong lines represent sampling-XANES spectra obtained within 400 ms after two flashes (predominant S_3 population) and three flashes (predominant S_0 population), respectively.

intact PSII (Haumann, Hundelt *et al.*, 1997; Razeghifard & Pace, 1997). The transient obtained upon flash 1 (Fig. 7, inset), where Mn oxidation occurs with $t_{1/2} \simeq 100$ µs, on the other hand, resembles a step function at the here-used resolution of 200 µs per point. For the first time, the $S_3 \rightarrow S_0$ transition was followed in real time using X-ray spectroscopy. That the rise time is close to 1 ms suggests that the Mn complex is in its most intact conformation (Haumann, Bögershausen *et al.*, 1997; Haumann, Hundelt *et al.*, 1997) in the here-used (partly dehydrated) XAS samples.

Time scans of the fluorescence changes which are caused by the flash that induces the oxygen-evolving transition $S_3 \rightarrow S_0$ (flash 3) were recorded with 200 µs per point at a series of excitation energies in the rising part of the Mn *K* edge. From these data, a time series of sampling-XANES spectra was constructed where the individual spectra are separated by only 500 µs in time (Fig. 8, symbols). The transient spectra obtained within 500 µs before flash 3 and at ~3 ms after this flash are very similar to those obtained by averaging of data within 400 ms before and after flash 3 (from fluorescence levels F^2 and F^3, see Fig. 2-ii, inset), suggesting that the structural and oxidation state changes closely follow the electron extraction by Tyr_Z^{ox}. The mechanistically particularly important question as to whether intermediate states are formed within the first 500 µs remains open at the presently achieved time resolution of 200 µs. The transient XANES spectra reflect the changes in edge shape and energy owing to the reduction (by four electrons from water) and structural rearrangement at the Mn atoms [lengthening of Mn—ligand distances (see Dau *et al.*, 2003), loss of one μ-oxo bridge and possibly protonation of another μ-oxo bridge] during the oxygen-evolving transition (Dau *et al.*, 2001; Dau & Haumann, 2003).

5. Conclusions

By tracking the structural and electronic changes at biological metal centers in real time, valuable information can be gained. A novel fluorescence-mode BioXAS technique is presented, termed sampling-XAS, which allows for the monitoring of state transitions and for the resolution of intermediates with microsecond to second time resolution at room temperature using water-containing non-crystalline metalloenzyme samples. By monitoring the structural changes directly at (almost) physiological conditions, potential ambiguities (crystal packing effects, cryo-artifacts *etc.*) can be avoided.

The manganese complex of PSII, which catalyses the formation of the atmospheric dioxygen, was used as a specifically well suited model system to explore the prospects and current limitations of the sampling-XAS technique. Preliminary room-temperature XANES and EXAFS spectra were obtained which represent the structure of the Mn complex acquired within milliseconds after population of the respective S state by laser-flash illumination. Furthermore, the time course of the oxygen-evolving transition was followed in real time with 200 µs resolution. In the future, similar experiments may extend the results obtained from our previous XAS investigations (Iuzzolino *et al.*, 1998; Meinke *et al.*, 2000; Dau *et al.*, 2001; Haumann, Grabolle *et al.*, 2002; Haumann, Pospisil

et al., 2002; Pospisil *et al.*, 2003; Dau & Haumann, 2003; Dau *et al.*, 2003; Magnuson *et al.*, 2004). Specifically we conclude:

(i) Room-temperature XAS at a high-flux undulator beamline is feasible even if highly oxidized metal centers are used which are particularly susceptible to X-ray photoreduction. By the employment of well adapted measuring protocols, any significant radiation-damage influence can be avoided.

(ii) The Mn complex is in its most intact conformation in our XAS samples in the majority of centers as indicated by the short rise time of the $S_3 \rightarrow S_0$ transition determined by analysis of the time course of X-ray transients. The stepping of the Mn complex through the catalytic cycle can be achieved by laser-flash illumination at the beamline.

(iii) It has been demonstrated that the sampling-XAS approach can facilitate determination of XANES and EXAFS spectra for intermediates of the S-state cycle.

(iv) The shown time-resolved XAS data on the $S_3 \rightarrow S_0$ transition, where Mn becomes reduced, represent a first step towards characterization of putative intermediate states with lifetimes in the microsecond range. Such intermediates may be related to formation and decay of the S_4 state during the process of oxygen evolution. By further improvement of these measurements and their extension into the EXAFS region, the direct monitoring in real time of the changes in electronic structure and nuclear geometry at the Mn complex during all four S transitions may become feasible. These experiments are expected to provide new structural and electronic information of high importance for the understanding of the mechanism of photosynthetic oxygen-evolution.

Financial support by the German BMBF (grant 05KS1KEA/6) and by the Deutsche Forschungsgemeinschaft (SFB 498, projects C6 and C8) is gratefully acknowledged. We thank the staff members at ID26 and M. Fünning for excellent technical assistance.

References

Adachi, S., Park, S. Y., Tame, J. R., Shiro, Y. & Shibayama, N. (2003). *Proc. Natl. Acad. Sci. USA*, **100**, 7039–7044.

Ankudinov, A. L., Ravel, B., Rehr, J. J. & Conradson, S. D. (1998). *Phys. Rev. B*, **12**, 7565–7576.

Ascone, I., Meyer-Klaucke, W. & Murphy, L. (2003). *J. Synchrotron Rad.* **10**, 16–22.

Dau, H., Dittmer, J., Iuzzolino, L., Schiller, H., Dörner, W., Heinze, L., Sole, V. A. & Nolting, H.-F. (1997). *J. Phys. IV*, **7**, 607–610.

Dau, H. & Haumann, M. (2003). *J. Synchrotron Rad.* **10**, 76–85.

Dau, H., Iuzzolino, L. & Dittmer, J. (2001). *Biochim. Biophys. Acta*, **1503**, 24–39.

Dau, H., Iuzzolino, L., Dittmer, J., Dörner, W. & Meyer-Klaucke, W. (1998). *Photosynthesis: Mechanism and Effects*, Vol. II, edited by G. Garab, pp. 1327–1330. Dordrecht: Kluwer.

Dau, H., Liebisch, P. & Haumann, M. (2003). *Anal. Bioanal. Chem.* **376**, 562–583.

Dau, H., Liebisch, H. & Haumann, M. (2004). *Phys. Chem. Chem. Phys.* **6**, 4781–4792.

Dekker, J. P., Plijter, J. J., Ouwehand, L. & van Gorkom, H. J. (1984). *Biochim. Biophys. Acta*, **767**, 176–179.

Della Longa, S. D., Ascone, I., Fontaine, A., Congiu Castellano, A. & Bianconi, A. (1994). *Eur. Biophys. J.* **23**, 361–368.

Dittmer, J., Iuzzolino, L., Dörner, W., Nolting, H.-F., Meyer-Klaucke, W. & Dau, H. (1998). *Photosynthesis: Mechanism and Effects*, Vol. II, edited by G. Garab, pp. 1339–1342. Dordrecht: Kluwer.

Ferreira, K. N., Iverson, T. M., Maghlaoui, K., Barber, J. & Iwata, S. (2004). *Science*, **303**, 1831–1838.

Grabolle, M., Haumann, M., Liebisch, P., Müller, C., Neisius, T., Meyer-Klaucke, W. & Dau, H. (2005). In preparation.

Haumann, M., Bögershausen, O., Cherepanov, D. A., Ahlbrink, R. & Junge, W. (1997). *Photosynth. Res.* **51**, 193–208.

Haumann, M., Grabolle, M., Neisius, T. & Dau, H. (2002). *FEBS Lett.* **512**, 116–120.

Haumann, M., Grabolle, M., Werthammer, M., Iuzzolino, L., Dittmer, J., Meyer-Klaucke, W., Neisius, T. & Dau, H. (2001). *PS2001 Proceedings*, Contribution S10-013, pp. 1–5. Collingwood: CSIRO Publishing.

Haumann, M., Hundelt, M., Jahns, P., Chroni, S., Bögershausen, O., Ghanotakis, D. & Junge, W. (1997). *FEBS Lett.* **410**, 243–248.

Haumann, M. & Junge, W. (1999). *Biochim. Biophys. Acta*, **1411**, 86–91.

Haumann, M., Müller, C., Liebisch, P., Iuzzolino, L., Dittmer, J., Grabolle, M., Neisius, T., Meyer-Klaucke, W. & Dau, H. (2004). *Biochemistry*. In the press.

Haumann, M., Pospisil, P., Grabolle, M., Müller, C., Liebisch, P., Solé, V. A., Neisius, T., Dittmer, J. & Dau, H. (2002). *J. Synchrotron Rad.* **9**, 304–309.

Hill, H. A. O., Sadler, P. J. & Thomson, A. J. (1999). *Metal Sites in Proteins and Models.* Berlin: Springer.

Iuzzolino, L., Dittmer, J., Doerner, W., Meyer-Klaucke, W. & Dau, H. (1998). *Biochemistry*, **37**, 17112–17119.

Joo, M. S., Tourillon, G., Sayers, D. E. & Theil, E. C. (1990). *Biol. Met.* **3**, 171–175.

Kamiya, N. & Shen, J. R. (2003). *Proc. Natl. Acad. Sci. USA*, **100**, 98–103.

Kleifeld, O., Frenkel, A., Martin, J. M. & Sagi, I. (2003). *Nature Struct. Biol.* **10**, 75–77.

Liang, W., Roelofs, T., Cinco, R. M., Rompel, A., Latimer, M., Yu, W., Sauer, K., Klein, M. P. & Yachandra, V. K. (2000). *J. Am. Chem. Soc.* **122**, 3399–3412.

Lützenkirchen-Hecht, D., Grundmann, S. & Frahm, R. (2001). *J. Synchrotron Rad.* **8**, 6–9.

Magnuson, A., Liebisch, P., Haumann, M., Högblom, J. E. B., Anderlund, M. F., Lomoth, R., Meyer-Klaucke, W. & Dau, H. (2004). *J. Bioinorg. Chem.* Submitted for publication.

Meinke, C., Solé, V. A., Pospisil, P. & Dau, H. (2000). *Biochemistry*, **39**, 7033–7040.

Messinger, J., Robblee, J. H., Bergmann, U., Fernandez, C., Glatzel, P., Visser, H., Cinco, R. M., McFarlane, K. L., Bellacchio, E., Pizarro, S. A., Cramer, S. P., Sauer, K., Klein, M. P. & Yachandra, V. K. (2001). *J. Am. Chem. Soc.* **123**, 7804–7820.

Moffat, K. (2003). *Faraday Discuss.* **122**, 65–77.

Ono, T., Nogushi, T., Inoue, Y., Kusunoki, M., Matsushita, T. & Oyanagi, H. (1992). *Science*, **258**, 1335–1337.

Pascarelli, S., Neisius, T., De Panfilis, S., Bonfim, M., Pizzini, S., Mackay, K., David, S., Fontaine, A., San Miguel, A., Itie, J. P., Gauthier, M. & Polian, A. (1999). *J. Synchrotron Rad.* **6**, 146–148.

Penner-Hahn, J. E. (1999). *Metal Sites in Proteins and Models: Redox Centres*, edited by H. A. O. Hill, P. J. Sadler and A. J. Thomson, pp. 1–36. Berlin: Springer.

Pospisil, P., Haumann, M., Dittmer, J., Solé, A. V. & Dau, H. (2003). *Biophys. J.* **84**, 1370–1386.

Rappaport, F., Blanchard-Desce, M. & Lavergne, J. (1994). *Biochim. Biophys. Acta*, **1184**, 178–192.

Razeghifard, M. R. & Pace, R. J. (1997). *Biochim. Biophys. Acta*, **1322**, 141–150.

Renger, G. & Hanssum, B. (1992). *FEBS Lett.* **299**, 28–32.

Ren, Z., Perman, B., Srajer, V., Teng, T. Y., Pradervand, C., Bourgeois, D., Schotte, F., Ursby, T., Kort, R., Wulff, M. & Moffat, K. (2001). *Biochemistry*, **40**, 13788–13801.
Richwin, M., Zaeper, R., Lützenkirchen-Hecht, D. & Frahm, R. (2001). *J. Synchrotron Rad.* **8**, 354–356.
Robblee, J. H., Cinco, R. M. & Yachandra, V. K. (2001). *Biochim. Biophys. Acta*, **1503**, 7–23.
Robblee, J. H., Messinger, J., Cinco, R. M., McFarlane, K. L., Fernandez, C., Pizarro, S. A., Sauer, K. & Yachandra, V. K. (2002). *J. Am. Chem. Soc.* **124**, 7459–7471.
Rutherford, A. W. & Faller, P. (2001). *Trends Biochem. Sci.* **26**, 341–344.
Scherk, C. G., Ostermann, A., Achterhold, K., Iakovleva, O., Nazikkol, C., Krebs, B., Knapp, E. W., Meyer-Klaucke, W. & Parak, F. G. (2001). *Eur. Biophys. J.* **30**, 393–403.
Schiller, H. & Dau, H. (2000). *J. Photochem. Photobiol. B*, **55**, 138–144.
Schiller, H., Dittmer, J., Iuzzolino, L., Doerner, W., Meyer-Klaucke, W., Sole, V. A., Nordstroem, T. & Dau, H. (1998). *Biochemistry*, **37**, 7340–7350.
Schotte, F., Lim, M., Jackson, T. A., Smirnov, A. V., Soman, J., Olson, J. S., Phillips, G. N. Jr, Wulff, M. & Anfinrud, P. A. (2003). *Science*, **300**, 1944–1947.
Scott, R. A. (2000). *Physical Methods in Bioinorganic Chemistry – Spectroscopy and Magnetism*, edited by L. Que Jr, pp. 465–504. Sausalito: University Science.
Scott, W. G. (2002). *Methods*, **28**, 302–306.
Shimizu, H., Park, S., Lee, D., Shoun, H. & Shiro, Y. (2000). *J. Inorg. Biochem.* **81**, 191–205.
Solé, V. A., Gauthier, C., Goulon, J. & Natali, F. (1999). *J. Synchrotron Rad.* **6**, 174–175.
Stoddard, B. L. (2001). *Methods*, **24**, 125–138.
Teo, B. K. (1986). *EXAFS: Basic Principles and Data Analysis*. Berlin: Springer.
Yachandra, V. K. (1995). *Methods Enzymol.* **246**, 638–678.
Yachandra, V. K., Guiles, R. D., McDermott, A. E., Cole, J. L., Britt, R. D., Dexheimer, S. L., Sauer, K. & Klein, M. P. (1987). *Biochemistry*, **26**, 5974–5981.
Zouni, A., Witt, H.-T., Kern, J., Fromme, P., Krauß, N., Saenger, W. & Orth, P. (2001). *Nature (London)*, **409**, 739–743.